

Chiral Exchange Bias due to Interlayer Dzyaloshinskii-Moriya Interactions in Canted Synthetic Antiferromagnets

Amalio Fernández-Pacheco^{1,2*}, Elena Vedmedenko^{3**}, Fanny Ummelen^{2,4}, Rhodri Mansell^{2,5},
Dorothée Petit², Russell P. Cowburn²

¹ SUPA, School of Physics and Astronomy, University of Glasgow, Glasgow G12 8QQ, United Kingdom

² Cavendish Laboratory, University of Cambridge. JJ Thomson Avenue, Cambridge CB3 0HE, United Kingdom

³ Institute of Applied Physics, University of Hamburg. Jungiusstr 11 20355 Hamburg, Germany

⁴ Technical University of Eindhoven. 5600 MB Eindhoven, The Netherlands

⁵ Department of Applied Physics, Aalto University School of Science. P.O. Box 15100, 00076 Aalto, Finland

* amalio.fernandez-pacheco@glasgow.ac.uk

** vedmeden@physnet.uni-hamburg.de

ABSTRACT

Magnetic interfacial Dzyaloshinskii-Moriya interaction (DMI) in multi-layered thin films can lead to exotic chiral spin states, of paramount importance for future spintronic technologies. Until now, interfacial DMI has been reported as an intralayer interaction, mediated via a paramagnetic heavy metal in systems lacking inversion symmetry. Here, we show how, by designing synthetic antiferromagnets with canted magnetization states, it is also possible to observe interface interlayer-DMI. This manifests in our structures as a room temperature in-plane biased hysteresis loop controlled by the magnetization direction of an interlayer-coupled perpendicularly magnetized layer. We further show how this interlayer chiral exchange bias can be reversed by simple external magnetic field sequences, and its magnitude tuned by the magnetic thickness of the layers. This work opens an unexplored avenue for the development of new spin chiral textures in multi-layered thin film systems.

Since its recent discovery, the interfacial Dzyaloshinskii-Moriya interaction (DMI) in ultra-thin multi-layered magnetic systems has been postulated to be a key constituent of future spintronic technologies^{1–3}. DMI is an antisymmetric exchange interaction occurring in systems lacking inversion symmetry that promotes chiral coupling between spins. This gives rise to ferromagnetic systems hosting topological spin textures such as skyrmions and chiral domain walls, with outstanding properties to store, transport and process magnetic information^{4–9}.

Interfacial DMI in an ultra-thin ferromagnetic (FM) layer comprises the coupling of spins \mathbf{S}_i and \mathbf{S}_j , mediated by a paramagnetic (PM) heavy metal atom l in a neighbouring layer (see left sketch in **Fig. 1a**), as described by the three-site Lévy-Fert model¹⁰. The DMI energy is expressed as $E_{DMI} = \mathbf{D}_{ij}(\mathbf{S}_i \times \mathbf{S}_j)$, where \mathbf{D}_{ij} is the Moriya vector, whose direction is dictated by symmetry rules¹¹. This interaction favours one sense of rotation of spins in the same FM layer, i.e. it is a chiral intralayer interaction. Very recently, the emergence of a non-negligible interlayer (IL) DMI between neighbour FM layers separated by a spacer has been predicted¹²: Following analogous arguments, an IL-DMI will lead to the chiral coupling of spins of different FM layers via PM atoms located in an IL between both FMs (see right sketch in **Fig. 1a**). However, due to the rapid decrease of the DMI interaction with distance and the requirement of a correct symmetry for a non-zero DMI, this effect has not been experimentally observed¹³. Here, we report a room-temperature chiral exchange bias in synthetic antiferromagnetic bilayers with canted magnetization states. By comparing experimental results with Monte Carlo (MC) simulations based on analytical calculations, we conclude that this bias is caused by the IL-DMI. The chiral nature of the interaction between layers allows us to reverse the bias by the application of simple magnetic field sequences. Moreover, the bias magnitude scales with the effective macrospin canting angle of the magnetization, revealing that a delicate balance between magnetic energies is required for this effect to manifest. The experimental discovery of the IL-DMI here reported opens a new route to investigate novel chiral spin textures in synthetic antiferromagnets, of great interest for future spintronic technologies.

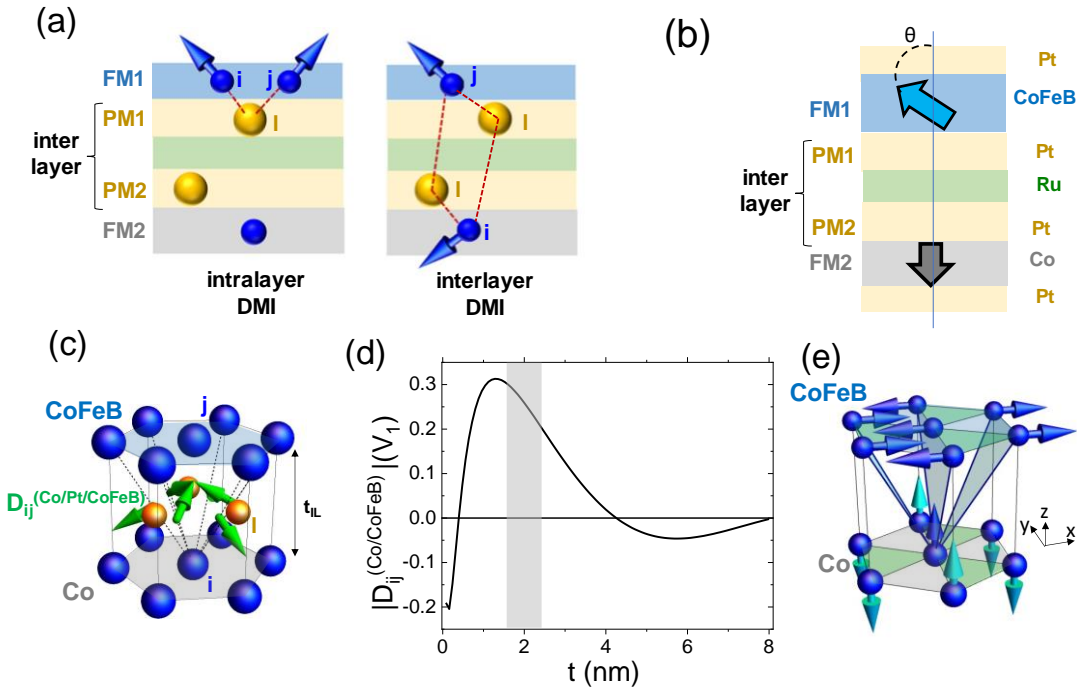


Fig. 1. Interlayer-DMI investigations in canted SAFs. (a) The presence of interfacial intralayer DMI (left) in ultra-thin FM layers results in spins of the same FM layer coupled via a PM, leading to chiral coupling and non-collinear spin configurations within the layer; the figure depicts this type of coupling for the top FM layer only. Analogously, an interlayer DMI effect (right) results in a chiral coupling between spins of two neighbouring layers separated by a spacer, mediated by PM atoms. (b) Schematic of the types of SAFs studied and their magnetic state at remanence in a macrospin approximation: two ultra-thin CoFeB (top) and Co (bottom) layers with Pt at the interfaces, separated by Ru to create AF between both FM layers via RKKY interaction. The two FM layers have different proximities to their corresponding SRT: whereas the Co layer remains out-of-plane due to its strong PMA, the CoFeB layer is just thicker than its SRT, so that, due to the AF coupling, it is canted with respect to the substrate plane. θ is the (polar) effective macrospin canting angle of this layer. (c) $D_{ij}^{(Co/Pt/CoFeB)}$ IL-DMI vectors (green) calculated via the 3-sites model for a CoFeB(j)/Pt(l)/Co(i) trilayer with hcp structure. The distance between magnetic atoms is the interlayer thickness (t_{IL}). (d) Analytical calculation of the dependence of the magnitude of the intralayer $D_{ij}^{(Co/Pt/CoFeB)}$ vector (in units of $V_1^{(Co/Pt/CoFeB)}$) as a function of the parameter t , describing the effective CoFeB thickness, for the SAFs under study. Grey area marks the equivalent thickness range investigated here. (e) Ground state spin configuration based solely on the IL-DMI, for a hcp trilayer with in-plane top and out-of-plane bottom magnetizations (no FM direct exchange considered). The IL-DMI leads to a well-defined sense of rotation (in this case anticlockwise) of spin direction for alternating top and bottom planes. Green (blue) triangles mark the energetically favourable bonds with the central spin, for the same (different) plane.

IL-DMI should result in chiral coupling between two FM layers separated by a spacer. However, this effect, if present, is expected to be weak in comparison with other magnetic interactions, and emerges in FM layers comprising spin configurations deviating from a perfect FM alignment, due to symmetry arguments¹². In order to investigate this interaction, we have studied SAF bilayers as depicted in **Fig. 1b**. These are formed by two ultra-thin magnetic layers made of Co and CoFeB, with a heavy metal (Pt) on both sides of the two layers providing perpendicular magnetic anisotropy (PMA) and acting as a source of interfacial DMI. A Ru spacer separates both layers, coupling them antiferromagnetically via Ruderman-Kittel-Kasuya-Yosida (RKKY) interactions¹⁴, where the Pt layers are also exploited to tune

the magnitude of the effective RKKY coupling¹⁵. The SAF is designed to be magnetically asymmetric, with bottom Co and top CoFeB layer thickness below or above (respectively) their corresponding spin reorientation (SRT) thickness. This, added to the RKKY antiferromagnetic (AF) coupling, leads to canted magnetization states at remanence and during switching¹⁶. Specifically, the samples studied here are chosen such that the Co layer is significantly thinner than its SRT, i.e. this layer is magnetically hard, with its magnetization strongly out-of-plane (z-direction). On the contrary, the CoFeB layer is slightly thicker than its SRT thickness, with shape anisotropy just slightly larger than its PMA (see Methods). Thus, CoFeB is a soft magnetic layer, presenting, in general, canted magnetization configurations, i.e. it has a non-negligible magnetization component along both in-plane and z directions¹⁶. **Fig. 1b** schematically shows a typical remanent state of the system in a macrospin approximation, where θ is the effective canting angle of CoFeB, formed by the magnetization vector of this layer with the substrate normal. Furthermore, the application of an in-plane magnetic field during growth breaks the symmetry during deposition, providing a moderate in-plane anisotropy along the field direction¹⁷; the CoFeB in-plane easy axis is referred as the x-direction in the manuscript.

To estimate the IL-DMI strength in our samples, the complete system is represented by three layers arranged in hcp stacking, with two magnetic atom layers separated a distance t_{IL} from each other by one layer of non-magnetic atoms (see **Fig. 1c**). The microscopic intralayer and interlayer DMI vectors \mathbf{D}_{ij} are then analytically calculated using the three-site model. For this, both bottom (representing Co) and middle (representing Pt) layers remain fixed, while the vertical position of the top layer (representing CoFeB) is increased a distance t with respect to its initial symmetric configuration. The IL-strength per effective bond $|\mathbf{D}_{ij}^{(Co/Pt/CoFeB)}|$ resulting from this procedure, is plotted as a function of t in **Fig. 1d**. This curve effectively accounts for the dependence of IL-DMI with CoFeB thickness and presents an oscillatory behaviour with t , as expected. For the experimental CoFeB thickness range considered (see dashed region), $|\mathbf{D}_{ij}^{(Co/Pt/CoFeB)}| \approx 0.2\text{-}0.3V_I$, with V_I the so-called spin-orbit parameter of the material defining the magnitude of the \mathbf{D}_{ij} vectors^{10,12}. For Co/Pt ultrathin films, $V_I \approx 0.06 \text{ eV/atom}$ ¹⁰, the same order of magnitude as $J^{(Co)}$, the direct exchange interaction of Co^{refs 18,19}. This leads to DMI values typically of a few meV/atom for Co/Pt interfaces²⁰, similar to our calculations for Co/Pt/CoFeB, due to the inversely proportional dependence of \mathbf{D}_{ij} with the distance vectors (see Methods). Analytical calculations therefore predict a non-negligible IL-DMI. **Fig. 1e** depicts the ground state of the unit cell of the system, in the case of IL-DMI as the only exchange coupling interaction, for the case of strong x-direction in-plane CoFeB and PMA Co layers, respectively: a dominating IL-DMI with anticlockwise rotation of spins in between layers, results in an alternating configuration of spins in both top and bottom layers along the x-direction. Further details of the modelling are provided in Methods.

The possible presence of IL-DMI has been investigated by making use of the magnetic field protocol schematically described in **Figs. 2(a-b)**, which exploits the different reversal behaviour of the two SAF layers under vector magnetic fields^{16,21}. In the first step (1), a strong (~0.4 T) B_z field is applied,

saturating both layers; this field is used to set the magnetic state of the Co layer for the rest of the field sequence, and leads to a magnetic canted state in the CoFeB layer at remanence (2). This initialization is followed by a moderate in-plane field hysteresis loop ($B_x < 30$ mT) (3). This magnetic field sequence is thus a minor loop used to probe the reversal of the canted free layer, while the out-of-plane layer remains fixed along the z-direction. As depicted in the figure, whereas standard magnetic energy terms are symmetric under inversion of the CoFeB magnetization, the presence of a significant IL-DMI between the two ferromagnetic layers, favouring one handedness, could potentially result in a biased hysteresis loop under such a field sequence. Moreover, the chiral nature of such an interaction is also expected to lead to a bias field with the same magnitude but opposite sign, for the two different B_z saturating field directions (compare the loops of **Figs. 2a** and **2b**). The perpendicular bias effect here described therefore constitutes a fingerprint of IL-DMI.

Figs. 2c-f show experimental evidence of this IL-DMI mediated effect for one of the samples investigated, with CoFeB hysteresis loops shifted by $B_{bias} \approx \pm 1.1$ mT for the two possible Co orientations. These measurements are performed using focused magneto-optical Kerr effect (MOKE), probing both M_z (polar MOKE) and M_x (longitudinal MOKE) components of the magnetization as a function of B_x fields, with both giving evidence of the bias. Analogous (bulk) vibrating sample magnetometer (VSM) measurements with two sets of perpendicular pick-up coils complement these measurements (Supplementary). Additional experiments in these and reference samples, where substrate plane and magnetic field become purposely misaligned, give further evidence of the asymmetric switching of the layers, and discard any non-negligible B_z offset as the source of the bias (Supplementary).

To understand the experimental results in detail, we have performed MC simulations using the atomistic model described in **Figs.1c-e**. The parameters that most accurately reproduce our measurements are obtained by comparing whole sets of M_z -vs- B_z experimental results with MC simulations that incorporate analytically-calculated intra- and inter- layer DMI vectors; these are obtained from systematically scanning the parameter space defined by changes in $V_1^{(Pt/CoFeB)}$ (see Methods). **Figs. 2g-j** show computational results obtained from MC simulations, using the same magnetic field protocol as in experiments. A good agreement between experiments and simulations is observed, with simulations reproducing qualitatively well both shape of experimental loops and the bias effect; opposite signs for B_{bias} for antiparallel Co magnetization states are also replicated.

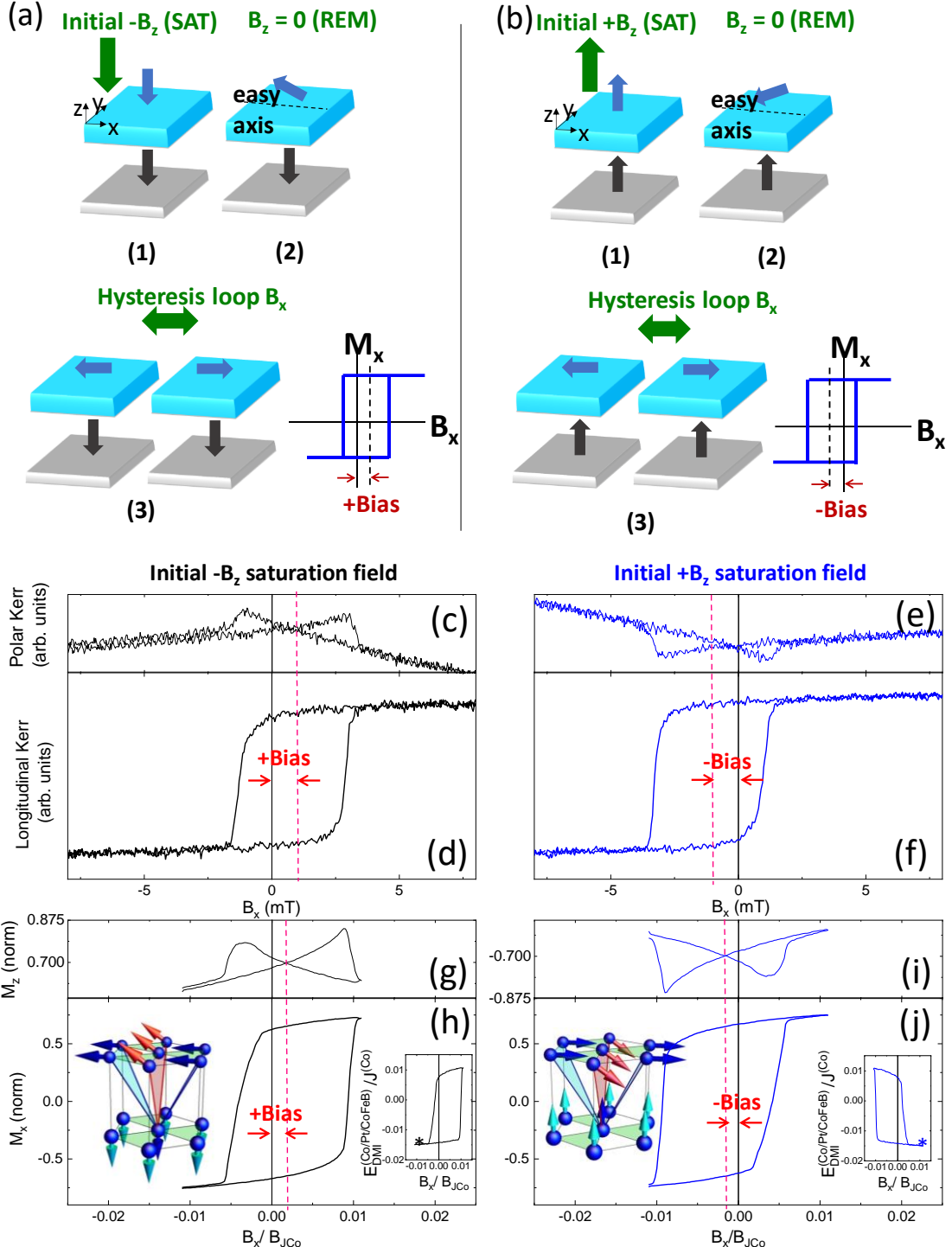


Fig. 2. Chiral exchange bias due to the IL-DMI. (a, b) Three step magnetic field sequence used to probe the effect. An opposite bias is observed depending on the direction the Co layer is initialized, revealing the chiral nature of the interlayer interaction. (c-f) Experimental realization of the effect for a sample with CoFeB thickness = 2.1 nm, where the magnetization components M_z (c,e) and M_x (d,f) are measured by Kerr effect under B_x magnetic fields, after negative (c,d) and positive (e,f) initial saturating B_z fields. The bias effect, obtained from the switching field (M_x) and peaks (M_z), is marked in red. (g-j) Monte Carlo atomistic simulations with $t = 2.1$ nm and $V_I^{(Pt/CoFeB)}/V_I^{(Co/Pt)} = 0.2$, reproducing the experiments. The bottom right inset shows the evolution of the IL-DMI energy during the hysteresis loop; an asterisk marks the most favourable state of the two under moderate B_x fields, based on this type of energy; this state is sketched in the bottom left inset, where red and blue arrows/triangles denote energetically unfavourable and favourable spins/bonds. B_x fields and IL_DMI are normalized with respect to $B_{JCo} = mJ^{(Co)}$ and $J^{(Co)}$, respectively, with m the magnetic moment of the system and $J^{(Co)}$ the direct intralayer exchange energy.

Fig. 3a shows snapshots of the MC simulations for Co pointing along the $+z$ direction: Overall, the magnetization process studied here follows the same mechanism previously reported for this range of anisotropies and RKKY coupling¹⁶, comprising the soft layer (CoFeB) reversing back and forth with B_x , while the hard (Co) layer remains unchanged because of its high PMA. The CoFeB layer reverses by acquiring a z -component antiparallel to Co, due to the AF RKKY coupling. However, and as expected from the shifted loops, simulations show a clear switching mechanism asymmetry between the branches of the hysteresis loop: For the case shown here, a single magnetic domain propagates either to the left or to the right, depending on the branch considered, whilst other simulations show instead processes comprising the expansion or contraction of magnetic domains for either of the two branches. The microscopic magnetic behaviour extracted from simulations is complex, as a result of the interplay of the different magnetic energies present: strong interlayer AF RKKY, forcing the M_z of CoFeB to be antiparallel to the one of Co; moderate CoFeB intralayer energies, namely in-plane anisotropy defining an easy axis, and intralayer-DMI favouring the clockwise rotation of spins across a domain wall; and moderate IL-DMI promoting chiral anticlockwise spin rotation in between Co and CoFeB layers. Furthermore, the reversal of CoFeB will be in reality strongly influenced by defects and inhomogeneities of the layers²²; despite this, the macroscopic bias observed experimentally indicates that a clear reversal asymmetry for both branches is present.

To unveil the physical grounds of this behaviour, the bottom right insets of **Figs. 2h-j** show the evolution of the IL-DMI energy $E_{\text{DMI}}^{(\text{Co/Pt/CoFeB})}$ for a hysteresis loop during CoFeB reversal, for the two possible z -directions of Co. The IL-DMI energy presents two plateaus at moderate B_x fields, and the switching in between both values is biased in field. Moreover, a contrary sign for either Co orientation, due to the chiral coupling between layers, is also confirmed. An asterisk in those graphs marks the state of the system energetically more favourable from an IL-DMI point of view, which is atomistically depicted in the bottom left insets. These sketches show the spin configuration for top CoFeB and bottom Co layers, where blue (red) arrows and polygons indicate respectively, the spins and bonds where the IL-DMI is energetically favourable (unfavourable). Since the IL-DMI chirality considered here promotes anticlockwise alignment of spins in between layers (**Fig. 1e**), unfavourable spins become more antiparallel to Co, because of the strong AF RKKY interaction. This type of spin configuration is observed in MC simulations, where the competition of non-zero intra- and inter-layer DMI results in CoFeB spin oscillations as those shown in **Fig. 3b**. Spin amplitude changes of up to 15% for S_x , with a period corresponding to a few spins are observed in simulations, with this behaviour dependent on the $/V_I^{(\text{Pt/CoFeB})}/ // V_I^{(\text{Co/Pt})}/$ ratio. The aforementioned sudden drop in IL-DMI energy during reversal results from the emergence of these spin modulations, manifested in experiments probing a much larger scale as a drop (increase) of the M_x (M_z) component. Whereas the IL-DMI would appear to be too weak to significantly change the intralayer magnetic ordering, due to the competition with a strong direct exchange and intralayer-DMI contributions, it can however be effective in competition with RKKY

coupling, co-defining the IL ordering. The subtle interplay of different magnetic energies in this system leads to non-collinear spin states at the microscopic level, a necessary ingredient to couple two FM

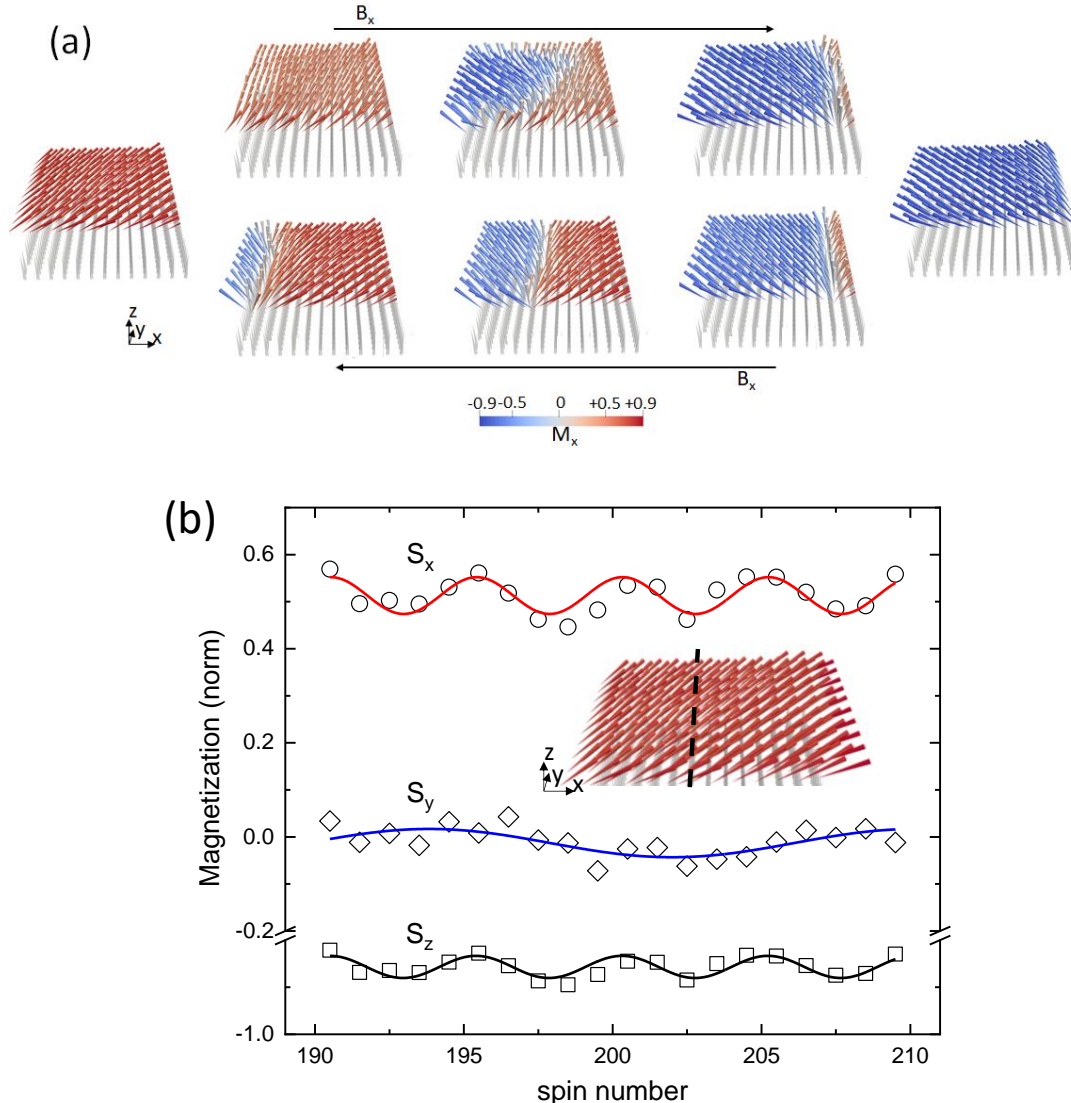


Fig. 3. Magnetization reversal of CoFeB layer under in-plane fields, studied by MC simulations (a) Snapshots of the simulations at remanence for a SAF with an effective CoFeB thickness $t = 2.1$ nm and Co pointing upwards. Forward (top) and backward (bottom) branches of the B_x hysteresis loop are included. Top spins in red and blue indicate the value of M_x for the top CoFeB layer during reversal. The grey bottom spins represent the Co layer along $+z$. The reversal process is asymmetric for both loop branches and occurs at different magnetic fields, resulting in a biased hysteresis loop. (b) Three components of the magnetization extracted from the simulations across the dashed line in the inset, for $B_x = 0$ and starting from negative fields. Oscillations of the three components reveal the presence of spin oscillations in the CoFeB layer during reversal.

layers with net magnetic moments via the IL-DMI¹².

Moreover, the bias field here observed shows a cosine angular dependence with in-plane fields, with a maximum/minimum for the x-direction, becoming negligible for fields along the y-direction

(Supplementary). The field-induced uniaxial in-plane anisotropy of the CoFeB layer reveals another key ingredient to observe the unidirectional IL-mediated bias.

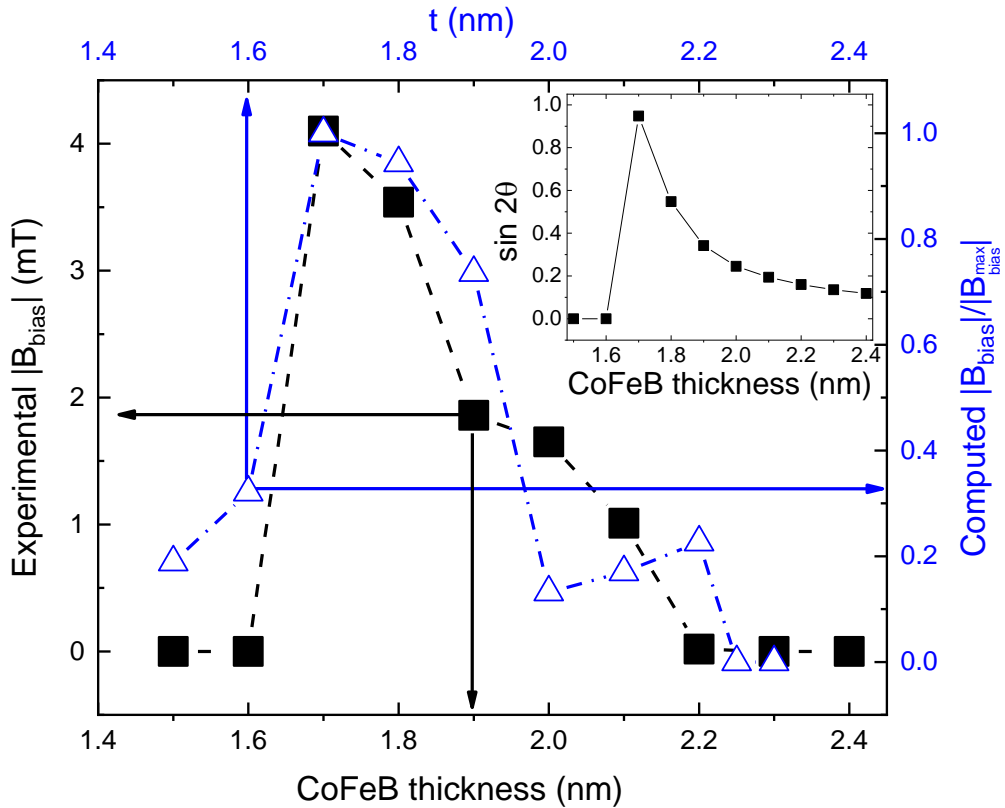


Fig. 4. Bias field dependence with CoFeB thickness. Experiments (left, bottom axes: black squares and dashed lines) show a sudden increase just after the SRT. Computed normalised bias from atomistic MC simulations (right, top axes: blue triangles and dash-dot lines), with t running for the same range as the experimental CoFeB thickness. The same behaviour is evidenced for experiments and simulations. The inset shows the degree of canting of the CoFeB layer as a function of its thickness, parametrized as $\sin 2\theta$, as extracted from macrospin MC simulations; only anisotropy and RKKY coupling interactions are considered.

The magnitude of the bias is well correlated with the magnetization effective degree of canting of the CoFeB layer, revealing that a low competing effective anisotropy is necessary to observe a bias effect.

To investigate further the range in which a measurable IL-DMI will manifest, we have studied the dependence of the chiral B_{bias} magnitude as a function of CoFeB thickness (left and bottom axes in **Fig. 4**) for the range 1.5 - 2.4 nm. A pronounced bias is measured for samples within an interval of 0.5 nm in this range, with a maximum value of 4 mT at 1.7 nm. For this type of SAF, this is also the regime where the CoFeB magnetization becomes canted¹⁶. The inset of **Fig. 4**. shows results from macrospin MC simulations for the SAFs under investigation, where only PMA, shape anisotropy and RKKY interactions have been considered, i.e. no IL-DMI is included. The function $\sin 2\theta$, parametrizing the effective degree of canting of a layer (when it is neither in-plane nor out-of-plane), presents an analogous dependence with CoFeB thickness as $|B_{\text{bias}}|$. The chiral bias can be therefore directly mapped by θ , the effective macrospin canting angle of the CoFeB layer (see **Fig. 1b**). In addition, right and top axes in **Fig. 4** shows the normalized $|B_{\text{bias}}|$ extracted from MC atomistic simulations, as a function of t , for the equivalent range of investigated CoFeB thickness. This corresponds to an interval of

$|V_I^{(Pt/CoFeB)}/V_I^{(Co/Pt)}|$ between -0.2 and +1.1 (Methods). An excellent agreement is observed between experiments and simulations, with both functions rising sharply after the nominal SRT CoFeB thickness, with a peak at 1.7 nm, and a drop to negligible values for thicknesses above 2.2 nm. We therefore observe the emergence of a chiral bias driven by the IL-DMI for CoFeB thicknesses just after its SRT, where non-collinear spin states are promoted by small effective anisotropy values, resulting in a net non-zero $E_{DMI}^{(Co/Pt/CoFeB)}$ ref²³.

The bias effect here reported is robust: we have observed it using several magnetometry techniques that probe different length scales, and for other sample series analogous to the ones shown in the main manuscript (Supplementary). Other perpendicular indirect exchange interactions²⁴ cannot account for the chiral nature of the observed effect. A crystalline texture substantially tilted with respect to the substrate plane, a possible source of perpendicular bias²⁵, is not a relevant factor in our samples (Supplementary). Furthermore, intra-layer DMI effects leading to asymmetric magnetization reversal processes have been only observed in laterally-patterned nanomagnets, and require the simultaneous application of orthogonal magnetic fields^{26,27}, in contrast to our experiments.

In conclusion, we report a room temperature chiral exchange bias in ultra-thin asymmetric synthetic antiferromagnetic bilayers that we associate to the presence of DMI across an interlayer. This effect is observed during the in-plane reversal of a canted magnetic layer, subject to strong AF coupling by a fixed perpendicular layer. The bias changes sign, depending on the direction of an initially-applied saturating perpendicular field, revealing a chiral indirect interaction. We complement experimental observations with MC simulations, confirming the IL-DMI as the driving mechanism. The bias is observed for a range of CoFeB thickness within a 0.5 nm range above its SRT, i.e. where non-collinear spin states are present. We expect IL-DMI to manifest as well in other ultra-thin SAF systems away from the SRT, where the magnetic reversal becomes dominated by areas with a low effective anisotropy, such as defects and layer inhomogeneities. The realization of systems integrating interlayer magnetic chiral interactions paves the way for the creation and manipulation of novel spin textures in three-dimensional spintronic multilayered systems^{28–30}.

ACKNOWLEDGEMENTS

This research has been funded by the European Union under the 7th FP, Contract No. 247368 (3SPIN), and under the Horizon 2020 research and innovation program under Grant Agreement No. 665095 (MAGicSky). AFP acknowledges support from an EPSRC Early Career Fellowship EP/M008517/1 and a Winton Fellowship. FU thanks the Erasmus Mobility program. We acknowledge fruitful discussions with Nicolas Jaouen, Stefan Stanesco and Aurelio Hierro-Rodríguez, as well as experimental support from Déraldo Sanz Hernández, Alexander Welbourne and Ian Farrer.

METHODS

Experimental details

The samples here studied were grown by DC magnetron sputtering, under base pressure of 7×10^{-8} mbar and a growth pressure of 8×10^{-3} mbar. Their structure is Ta(4.0 nm)/Pt(10.0 nm)/Co(1 nm)/Pt(0.5 nm)/Ru(1.0 nm)/Pt(0.5 nm)/CoFeB(1.6-2.4 nm)/Pt(2.0 nm)/Ta(2.0 nm). The surface PMA of Co and CoFeB layers, determined by growing single layers with analogous structure, are 1.2 mJ/m^2 and 0.7 mJ/m^2 . This corresponds to SRT thicknesses of $\approx 1.95 \text{ nm}$ and 1.55 nm , respectively, when the effective anisotropy $K_{\text{eff}} = 2K_s/t - 0.5 \mu_0 M_s^2$ becomes zero. RKKY coupling is created by a 1 nm Ru layer, which corresponds to the first AF peak, and tuned by the Pt at both sides. For 0.5 nm of Pt, this corresponds to an AF surface energy of $J_{\text{RKKY}}^{(\text{Co/Ru/CoFeB})} = -0.08 \text{ mJ/m}^2$. A magnetic field during growth of $\approx 100 \text{ mT}$ is applied during the sputtering process, resulting in a moderate in-plane anisotropy for the CoFeB layer along the field direction, measured to be up to $1.8 \times 10^3 \text{ J/m}^3$.

Magnetic characterization

The samples under investigation were studied using focused magneto-optical Kerr effect, with a 3.5 mW laser Gaussian spot of FWHM $\approx 5 \text{ } \mu\text{m}$ and wavelength = 635 nm. To probe both M_z and M_x components of the samples, two different setups were used, with either normal or 45 degree-incidence geometries. Optical analyzer and quarter-wave plate angles were tuned to detect either Polar or Longitudinal Kerr signals, respectively. Kerr experiments results were complemented with bulk-magnetometry VSM measurements in representative samples (Supplementary), probing an area of $\approx 5 \times 5 \text{ mm}^2$. Two set of coils measuring both magnetization components were used, confirming Kerr results.

Modelling

The IL-DMI effect is modelled using FM₁/PM/FM₂ atomistic trilayers with hcp stacking, as described in the main text. Each of the magnetic layers is represented by a single monolayer of Heisenberg spins S_i and S_j at atomic positions \mathbf{R}_i and \mathbf{R}_j . The spin-orbit parameters for the bottom and top layers are defined as $V_1^{(\text{Co/Pt})}$ and $V_1^{(\text{Pt/CoFeB})}$, respectively, and between layers as $V_1^{(\text{Co/Pt/CoFeB})}$. Microscopic DMI vectors within and in-between layers have been then obtained on the basis of the three-sites model¹⁰:

$$D_{ijl}(\mathbf{R}_{li}, \mathbf{R}_{lj}, \mathbf{R}_{ij}) = -V_1 \frac{\sin(k_F(R_{li}+R_{lj}+R_{ij})+(\pi/10)Z_d)(\mathbf{R}_{li} \cdot \mathbf{R}_{lj})(\mathbf{R}_{li} \times \mathbf{R}_{lj})}{|R_{li}|^3 |R_{lj}|^3 R_{ij}}, \quad (1)$$

where \mathbf{R}_{li} , \mathbf{R}_{lj} are the distance vectors from the impurity l to the corresponding FM atom sites i and j , and \mathbf{R}_{ij} the distance vector between these FM sites. The parameter $V_1 = \frac{135\pi}{32} \frac{\lambda_d \Gamma^2}{E_F^2 k_F^3} \sin\left(\frac{\pi}{10} Z_d\right)$ refers to the material specific quantity defining the DMI strength. Hereby, k_F and E_F are the Fermi wave vector and energy respectively, λ_d is the spin-orbit coupling parameter, Γ the interaction parameter between the localized spins and the spins of conduction electrons, and Z_d the number of d-electrons.

An effective DMI vector of a given ij atomic pair can be described by a sum over all PM impurities l ^{10,12}:

$$\mathbf{D}_{ij}^{eff} = \sum_l \mathbf{D}_{ijl}(\mathbf{R}_{il}, \mathbf{R}_{lj}, \mathbf{R}_{ij}) \quad (2)$$

Next-nearest neighbour ij , il , and jl pairs are considered in the calculations. Complementing analytical calculations, atomistic MC simulations have been performed using the same methodology as in¹². The sample modelling is based on experiments, using typical parameters of Co-based alloys³¹: A strong PMA is included for the bottom Co layer, $K_{eff}^{(Co)} \approx K_z^{(Co)} \approx 0.7 J^{(Co)}$. The top CoFeB layer is close to the SRT, $K_z^{(CoFeB)} \approx 0$. Additionally, we introduce an additional in-plane anisotropy in this layer to mimic experiments: $K_x^{(CoFeB)} \approx 0.4 J^{(CoFeB)}$. The FM intralayer exchange interaction for both layers is set as $J^{(CoFeB)}/J^{(Co)} = 0.5$ and the AF RKKY coupling between both layers as $J_{RKKY}^{(Co/CoFeB)} = -0.1 J^{(Co)}$.

The complex polycrystalline and amorphous crystallographic structure of the sputtered layers, added to unknown spin-orbit parameters, makes it challenging to estimate the DMI values of the samples. This is added to the fact that V_I will have different values for Co/Pt, Pt/CoFeB and Co/Pt/CoFeB interfaces. To tackle this, and taking into account that the Co/Pt/Ru/Pt/CoFeB interface is nominally the same for all samples investigated (i.e. it is only the CoFeB thickness that changes from sample to sample), we fix $V_I^{(Co)} = 0.06$ eV/atom¹⁰ for both $V_I^{(Co/Pt)}$ and $V_I^{(Co/Pt/CoFeB)}$, with $V_I^{(Co)}/J^{(Co)} \approx 1$ ref. 19. This makes $V_I^{(Pt/CoFeB)}$ the only spin-orbit parameter changing with CoFeB thickness in the calculations. Because the $V_I^{(Pt/CoFeB)}$ vs t_{IL} function is unknown, all microscopic intra- and inter-layer $|\mathbf{D}_{ij}|$ are calculated on the basis of the three-sites model¹², for $V_I^{(Pt/CoFeB)}$ values across the range 0.1-1 $J^{(Co)}$. These $|\mathbf{D}_{ij}|$ values are subsequently incorporated into MC simulations, allowing us to compare hysteresis loops obtained from them with experimental results. Specifically, we simultaneously compare simulations with polar Kerr loops obtained under strong B_z fields for the whole thickness range of samples studied, finding the curve of $V_I^{(Pt/CoFeB)}$ vs t that reproduces best key features of the experimental loops (Supplementary). The analysis here performed permits us to identify the sets of spin-orbit parameters that result in magnetic loops having a good agreement with experimental data for different thickness of CoFeB, modelling the thickness dependence of the chiral bias.

Estimation of the IL-DMI energy from the Bias Field

Since the IL-DMI is considered as the only symmetry-breaking source in the system, $|\mathbf{B}_{bias}|$ can be identified with the effective strength of the IL-DMI. Hence, e.g. a bias of 1 mT for the 2.1 nm thick CoFeB corresponds to an effective energy of 10^{-4} meV/atom, given by $E_{DM}^{(Co/Pt/CoFeB)} = m/|\mathbf{B}_{bias}| \approx 2 \mu_B$ /atom $\times 1$ mT $\approx 10^{-4}$ meV/atom, with m the magnetic atomic moment, expressed in units of the Bohr magneton μ_B . This compares with the energy extracted from simulations (right insets of **Figs. 2h-j**), with $E_{DM}^{(Co/Pt/CoFeB)} \sim 0.001 J^{(Co)} \approx 2 \times 10^{-2}$ meV/atom, if $J^{(Co)} \approx 20$ meV/atom is considered¹⁸. The difference between the effective experimental value and the one obtained from theory is expected, due

to the complex experimental system investigated, comprising polycrystalline/amorphous sputtered samples and rough interfaces, in contrast with the model, where a perfect crystalline hcp structure has been considered.

Macrospin simulations

Macrospin MC simulations were carried out to determine the effective canting angle of the CoFeB layer as a function of its thickness, for the SAF under investigation (inset Fig. 4). PMA, in-plane shape anisotropy and RKKY AF coupling were considered. The parameters used were extracted from experiments. PMA: $K_s^{(Co)} = 1.2 \text{ mJ/m}^2$, $K_s^{(CoFeB)} = 0.7 \text{ mJ/m}^2$. In-plane volume anisotropy: $K_v^{(CoFeB)} = 1.8 \times 10^2 \text{ J/m}^3$. Spontaneous magnetization: $M_s^{(Co)} = 1.4 \times 10^6 \text{ A/m}$, $M_s^{(CoFeB)} = 1.2 \times 10^6 \text{ A/m}$. $J_{RKKY}^{(Co/Ru/CoFeB)} = -0.08 \text{ mJ/m}^2$.

REFERENCES

1. Wiesendanger, R. Nanoscale magnetic skyrmions in metallic films and multilayers: a new twist for spintronics. *Nat. Rev. Mater.* **1**, 16044 (2016).
2. Hellman, F. *et al.* Interface-induced phenomena in magnetism. *Rev. Mod. Phys.* **89**, 025006 (2017).
3. Sander, D. *et al.* The 2017 Magnetism Roadmap. *J. Phys. D. Appl. Phys.* **50**, 363001 (2017).
4. Woo, S. *et al.* Observation of room-temperature magnetic skyrmions and their current-driven dynamics in ultrathin metallic ferromagnets. *Nat. Mater.* **15**, 501–506 (2016).
5. Boulle, O. *et al.* Room-temperature chiral magnetic skyrmions in ultrathin magnetic nanostructures. *Nat. Nanotechnol.* **11**, 449–454 (2016).
6. Yu, G. *et al.* Room-Temperature Skyrmions in an Antiferromagnet-Based Heterostructure. *Nano Lett.* **18**, 980–986 (2018).
7. Maccariello, D. *et al.* Electrical detection of single magnetic skyrmions in metallic multilayers at room temperature. *Nat. Nanotechnol.* **13**, 233–237 (2018).
8. Jué, E. *et al.* Chiral damping of magnetic domain walls. *Nat. Mater.* **15**, 272–277 (2015).
9. Ryu, K.-S., Thomas, L., Yang, S.-H. & Parkin, S. Chiral spin torque at magnetic domain walls. *Nat. Nanotechnol.* **8**, 527–533 (2013).
10. Levy, P. M. & Fert, A. Anisotropy induced by nonmagnetic impurities in Cu Mn spin-glass alloys. *Phys. Rev. B* **23**, 4667–4690 (1981).
11. Crépieux, A. & Lacroix, C. Dzyaloshinsky–Moriya interactions induced by symmetry breaking at a surface. *J. Magn. Magn. Mater.* **182**, 341–349 (1998).
12. Vedmedenko, E. Y., Arregi, J. A., Riego, P. & Berger, A. Interlayer Dzyaloshinskii–Moriya interactions. *arXiv:1803.10570v2* (2018).
13. While writing this manuscript, we became aware of this other publication reporting experimental evidence of interlayer-DMI: Han, D.-S. *et al.* Chiral magnetic interlayer coupling in synthetic antiferromagnets: Han, D.-S. *et al.* Chiral magnetic interlayer coupling in synthetic antiferromagnets. *arXiv:1809.01080v1* (2018).
14. Wiese, N. *et al.* Antiferromagnetically coupled CoFeB/Ru/CoFeB trilayers. *Appl. Phys. Lett.* **85**, 2020 (2004).
15. Lavrijsen, R. *et al.* Tuning the interlayer exchange coupling between single perpendicularly magnetized CoFeB layers. *Appl. Phys. Lett.* **100**, 052411 (2012).
16. Ummelen, F. C. *et al.* Controlling the canted state in antiferromagnetically coupled magnetic bilayers close to the spin reorientation transition. *Appl. Phys. Lett.* **110**, (2017).
17. Fernández-Pacheco, A. *et al.* Controllable nucleation and propagation of topological magnetic solitons in CoFeB/Ru ferrimagnetic superlattices. *Phys. Rev. B - Condens. Matter Mater. Phys.* **86**, (2012).
18. Dupé, B., Hoffmann, M., Paillard, C. & Heinze, S. Tailoring magnetic skyrmions in ultra-thin transition metal films. *Nat. Commun.* **5**, 4030 (2014).
19. Perini, M. *et al.* Domain walls and Dzyaloshinskii–Moriya interaction in epitaxial Co/Ir(111) and Pt/Co/Ir(111). *Phys. Rev. B* **97**, 184425 (2018).
20. Yang, H., Thiaville, A., Rohart, S., Fert, A. & Chshiev, M. Anatomy of Dzyaloshinskii–Moriya Interaction at Co / Pt Interfaces. *Phys. Rev. Lett.* **115**, 267210 (2015).

21. Fernández-Pacheco, A. *et al.* Dynamic selective switching in antiferromagnetically-coupled bilayers close to the spin reorientation transition. *Appl. Phys. Lett.* **105**, (2014).
22. Lee, J.-H. *et al.* Domain imaging during soliton propagation in a 3D magnetic ratchet. *SPIN* **03**, 1340013 (2013).
23. Ślęzak, T. *et al.* Noncollinear Magnetization Structure at the Thickness-Driven Spin-Reorientation Transition in Epitaxial Fe Films on W(110). *Phys. Rev. Lett.* **105**, 027206 (2010).
24. Ives, A. J. R., Bland, J. A. C., Hicken, R. J. & Daboo, C. Oscillatory biquadratic coupling in Fe/Cr/Fe(001). *Phys. Rev. B* **55**, 12428–12438 (1997).
25. Won, C. *et al.* Symmetry-Breaking Induced Exchange Bias in Ferromagnetic Ni-Cu-Co and Ni-Fe-Co Sandwiches Grown on a Vicinal Cu(001) Surface. *Phys. Rev. Lett.* **99**, 077203 (2007).
26. Pizzini, S. *et al.* Chirality-Induced Asymmetric Magnetic Nucleation in Pt/Co /AlOx Ultrathin Microstructures. *Phys. Rev. Lett.* **113**, 047203 (2014).
27. Han, D. S. *et al.* Asymmetric hysteresis for probing Dzyaloshinskii-Moriya interaction. *Nano Lett.* **16**, 4438–4446 (2016).
28. Lavrijsen, R. *et al.* Magnetic ratchet for three-dimensional spintronic memory and logic. *Nature* **494**, (2013).
29. Fernández-Pacheco, A. *et al.* Three dimensional nanomagnetism. *Nat. Commun.* **8**, 15756 (2017).
30. Legrand, W. *et al.* Hybrid chiral domain walls and skyrmions in magnetic multilayers. *Sci. Adv.* **4**, 0415 (2018).
31. Eyrich, C. *et al.* Exchange stiffness in thin film Co alloys. *J. Appl. Phys.* **111**, 07C919 (2012).